

DeSPITE: Exploring Contrastive Deep Skeleton-Pointcloud-IMU-Text Embeddings for Advanced Point Cloud Human Activity Understanding

Thomas Kreutz¹ Max Mühlhäuser¹ Alejandro Sanchez Guinea²

¹ Telekooperation Lab, Technical University Darmstadt

² NTT DATA, Luxembourg

{kreutz@tk, max@informatik}.tu-darmstadt.de, alejandro.guinea@global.ntt

Abstract

Despite LiDAR (Light Detection and Ranging) being an effective privacy-preserving alternative to RGB cameras to perceive human activities, it remains largely underexplored in the context of multi-modal contrastive pre-training for human activity understanding (e.g., human activity recognition (HAR), retrieval, or person re-identification (RE-ID)). To close this gap, our work explores learning the correspondence between LiDAR point clouds, human skeleton poses, IMU data, and text in a joint embedding space. More specifically, we present DeSPITE, a Deep Skeleton-Pointcloud-IMU-Text Embedding model, which effectively learns a joint embedding space across these four modalities. At the heart of our empirical exploration, we have combined the existing LIPD and Babel datasets, which enabled us to synchronize data of all four modalities, allowing us to explore the learning of a new joint embedding space. Our experiments demonstrate novel human activity understanding tasks for point cloud sequences enabled through DeSPITE, including Skeleton \leftrightarrow Pointcloud \leftrightarrow IMU matching, retrieval, and temporal moment retrieval. Furthermore, we show that DeSPITE is an effective pre-training strategy for point cloud HAR through experiments in MSR-Action3D and HMPear.

1. Introduction

A key challenge in multi-modal human activity understanding tasks, such as human activity recognition (HAR), human pose estimation (HPE), retrieval, or person re-identification (RE-ID) “in the wild” is obtaining paired sensor data for each individual in a multi-person scene (e.g., IMU with human poses, point clouds, or RGB videos). Prior work has studied RGB-IMU matching for identity-aware tracking/RE-ID [4, 20], RGB-IMU matching for video retrieval [39], and IMU-Skeleton Pose matching [57] to correct IMU drift in multi-modal HPE. However, existing

methods primarily focus on RGB-centric modalities, limiting applicability to privacy-sensitive scenarios like healthcare and surveillance, where RGB cameras may not be able to be deployed.

To address privacy concerns, silhouette masks [37, 38] or skeletons [1] have been proposed to anonymize detected individuals from RGB video. While effective, these anonymization techniques still come with the limitation that they require post-processing and short-term storage of the raw RGB data. In contrast, LiDAR is a privacy-preserving alternative, with proven capabilities for multi-modal HAR (e.g., [29, 61]) and HPE (e.g., [24, 48]). However, matching skeleton or IMU signals to LiDAR-based point cloud sequences is underexplored.

Beyond matching, recent advances in multi-modal contrastive learning, such as ImageBind [15], IMU2CLIP [39], BabelTower [8], MotionCLIP [54], or LAVIMO [63] have demonstrated the power and benefits of cross-modal alignment for human activity understanding. These models learn a shared embedding space, enabling cross-modality matching, retrieval, and effective neural network pre-training for downstream tasks. Despite their success, they all use RGB data as a main visual modality to bind the learned representations. Extending this line of research, our paper asks the important research question *What happens if we only depend on LiDAR in multi-modal contrastive learning as the main visual modality?*, which has not been studied before.

We present DeSPITE, a Deep Skeleton-Pointcloud-IMU-Text Embedding model, which is illustrated in Figure 1. Inspired by CLIP [46], ImageBind [15], and IMU2CLIP [39], DeSPITE learns a shared embedding space with a contrastive loss based on InfoNCE [41] between paired sequences of point cloud \leftrightarrow skeleton \leftrightarrow IMU \leftrightarrow text data. Unlike prior works leveraging frozen text or RGB data embeddings as a binding modality (e.g., IMU2CLIP [39], MotionCLIP [54], LAVIMO [63]), our primary goal is not to demonstrate modality alignment to text. Instead, we present novel applications for point cloud-based human

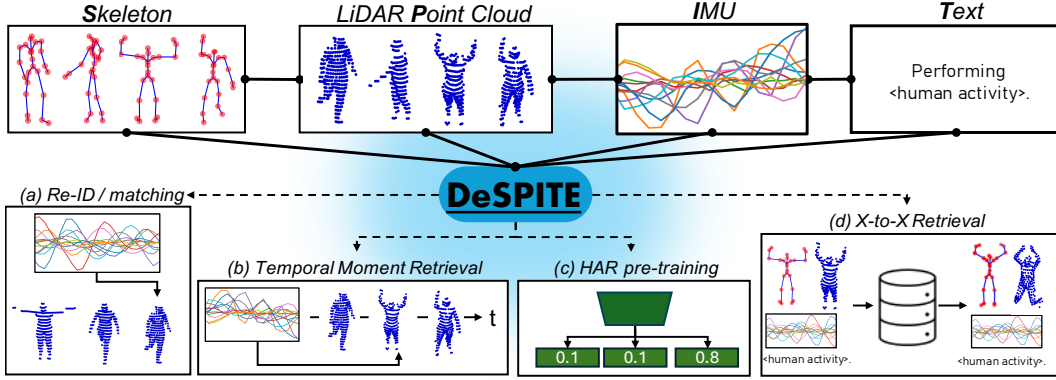


Figure 1. DeSPITE links different data modalities that represent human activities and, therefore, have a natural correspondence into a joint embedding space. As a result, DeSPITE enables tasks that depend on this correspondence that were not possible before.

activity sequences that were not possible before, enabled by unifying these modalities into a joint embedding space. Furthermore, while our primary focus is on enabling novel cross-modal retrieval and matching tasks, we find that DeSPITE also serves as an effective pre-training method for HAR, demonstrating improvements over uni-modal baselines. Finally, to understand the contribution of each modality to the joint embedding space, we train several DeSPITE variants (DeSPIE, DeSPE, etc.), evaluating their individual impact on cross-modal matching, retrieval, and HAR performance.

As described in Figure 1, after successful alignment in a shared embedding space, DeSPITE and its variants (e.g., DeSPIE) allow novel and very useful applications between point cloud, IMU, and skeleton data: (a) Person Re-ID by matching a snippet of, e.g., IMU data to the correct point cloud snippet, or a skeleton snippet to point cloud sequences, (b) Temporal moment retrieval/search in a video with skeletons, IMU, or a point cloud as query, (c) pre-training modality specific encoders for human activity recognition, and (d) retrieval of each modality through each modality from a large motion database.

To train and evaluate DeSPITE, we construct LIPD-Babel, a dataset aligning point clouds, IMU, skeletons, and text by integrating the LIPD dataset [48] with the text annotations from Babel [45]. LIPD-Babel enables two key evaluations: (1) LIPD-Babel-v1 for cross-modal matching and retrieval, demonstrating DeSPITE and DeSPIE’s ability to align point clouds, skeletons, and IMU signals, and (2) LIPD-Babel-v2 for contrastive pre-training, where DeSPITE and DeSPIE improve single-modality HAR, surpassing SOTA on HMPEAR [29] and MSR-Action3D [27].

Our contributions are as follows. (i) **DeSPITE**: A Deep Skeleton-Pointcloud-IMU-Text Embedding model that enables cross-modal matching and retrieval tasks between point clouds, IMU, and skeletons, unlocking applications that were previously impossible, and we will release the

resulting pre-trained encoders, code, and data for future research. (ii) We show that DeSPITE is an effective contrastive pre-training strategy for single-modality HAR, demonstrating new state-of-the-art performance. (iii) LIPD-Babel, a new dataset for privacy-preserving multi-modal learning, with versions LIPD-Babel-v1 tailored for matching, retrieval tasks, and LIPD-Babel-v2 tailored for HAR.

2. Related Work

2.1. Multi-Modal Contrastive Learning for Human Activity Understanding

Recent works have explored unified embedding spaces across sensor modalities. ImageBind [15] binds six modalities using image-text pairs, while IMU2CLIP [39] and MotionCLIP [54] align IMU and skeleton data with CLIP’s image-text space. LAVIMO [63] improves skeleton-video-text retrieval, and BabelTower [8] incrementally aligns six sensing modalities, reducing reliance on RGB. Unlike these works, we focus exclusively on privacy-preserving modalities, introducing LiDAR into a joint embedding space with IMU and skeletons. This enables novel retrieval tasks (LiDAR↔IMU, LiDAR↔Skeleton) and serves as an effective pre-training strategy for point cloud-based HAR.

2.2. Pre-Training for Point Cloud Human Activity Recognition

While countless general purpose embedding models and foundation models have emerged in the last years for RGB images/videos, natural language, or audio (e.g., ImageBind [15], DinoV2 [42], SAM2 [47], CLIP [46], BERT [9]), pre-trained general-purpose models for (LiDAR) point cloud HAR do not exist yet due to a lack of the same amount of data. To this day, pre-training mainly happens through self-supervision on a small number of datasets or the same dataset before fine-tuning for point cloud HAR. Self-supervision includes temporal order prediction from

shuffling in [53, 58], contrastive learning on masked sequences [18, 52], temporal structure prediction [51], or knowledge distillation [64]. All these methods have been shown to improve the performance after fine-tuning for HAR compared to training from scratch. Different from these works, we show that multi-modal contrastive learning between point clouds and other closely related modalities (i.e., skeleton pose and IMU data) leads to improved HAR performance after fine-tuning, showing new possibilities for future research in point cloud HAR.

2.3. Cross-Modal Matching and Retrieval between Modalities

Cross-modal matching assigns a data point from one modality to its correct counterpart in another. Key applications include audio-visual association [17, 23], IMU-based matching to human pose, RGB, or silhouette masks [37, 39, 57], or text-to-motion retrieval [44, 63]. Person Re-ID via IMU signals has been explored in RGB videos [4, 28], silhouette masks [37, 38], and skeletons [1, 57]. Retrieval tasks also exist between skeletons and text [44], skeletons and RGB [63], and IMU and RGB [39], with prior works exploring temporal moment retrieval and database retrieval.

However, LiDAR-based cross-modal retrieval remains largely unexplored. Our work extends these approaches by aligning LiDAR, IMU, and skeleton data, enabling novel retrieval tasks such as LiDAR↔Skeleton and LiDAR↔IMU. We further extend IMU interpretability via RGB video retrieval [39] to point cloud and skeleton retrieval, unlocking a new effective way to interpret IMU signals.

2.4. Datasets for LiDAR Point Cloud Human Activity Recognition

Early point cloud HAR datasets, like MSR-Action3D [27] and NTU-RGB+D [30, 50] are derived from depth maps and have been foundational in advancing state-of-the-art methods in the field. Datasets with real LiDAR point clouds of human activities are rare. One of the only datasets for human activity recognition are HuCenLife [61], and the recent HMPEAR [29] and MM-Fi [62] datasets. Motivated by multi-modal LiDAR and IMU-based HPE, several datasets have been proposed recently, such as LidarCap [24] and LIPD [48]. In particular, LIPD is a large-scale dataset with human motions of LiDAR point clouds, human skeletons, and IMU data, but without activity annotations. It is a mix of synthetic and real data, where a big part comes from AMASS [36], a large-scale human motion capture dataset. On top of AMASS, Babel [45] and HumanML3D [16] added natural language annotations. For our study, we combine LIPD with its corresponding subset in AMASS to a new dataset, LIPD-Babel, which enriches LIPD through partial human activity annotations. This leads to a large pre-training data resource between human skeletons, IMU,

LiDAR point clouds, and text, which we can leverage to explore contrastive learning between these modalities.

3. Method

3.1. Problem Statement

The goal of this work is to learn a joint embedding space that aligns human motion observed through different privacy-preserving modalities. More specifically, we present DeSPITE, a Deep Skeleton-Pointcloud-IMU-Text Embedding model, which effectively learns a joint embedding space across these four respective modalities through a contrastive loss based on InfoNCE [41].

We train several versions of DeSPITE, where we vary the number of modalities (DeSIE, DeSPE, DePIE, DePITE, ...). When all modalities are used, the text embeddings of CLIP serve as a binding modality, which has been shown to be effective in several recent related works for modalities that capture human motion, such as IMU data and human skeletons [1, 15, 35, 39, 54, 63].

We want to emphasize that the primary goal of DeSPITE is *not* to show that we can bind skeleton, point cloud, or IMU data to CLIP text embeddings (this has been demonstrated before with, e.g., ImageBind [15], IMU2CLIP [39], MotionCLIP [54], or BabelTower [8]). Instead, our main goal is to present several novel unexplored applications for human activity point cloud sequences that emerge when we unify these modalities into a joint embedding space.

3.2. Learning Deep Skeleton-Pointcloud-IMU-Text Embeddings (DeSPITE)

Human motions represented through LiDAR point clouds, IMU time series, and human pose skeleton data have an inherent correspondence. We leverage this property to learn a joint embedding space where similar sequences of human motions are close and different sequences are far apart.

Given a point cloud sequence $X_{pc} := \{pc_1, \dots, pc_T\}$, with $pc_i \in \mathbb{R}^{N \times 3}$, an IMU sequence $X_{imu} := \{imu_1, \dots, imu_T\}$, with $imu_i \in \mathbb{R}^C$, and a human pose sequence $X_{pose} := \{pose_1, \dots, pose_T\}$, with $pose_i \in \mathbb{R}^{24 \times 3}$ representing 3D positions of 24 skeletal joints, we aim to train neural networks to encode X_{pc} , X_{imu} , and X_{pose} into a shared embedding space. We denote these neural networks as encoders

$$\begin{aligned} f_{pc} : \mathbb{R}^{T \times N \times 3} &\rightarrow \mathbb{R}^e, \\ f_{imu} : \mathbb{R}^{T \times C} &\rightarrow \mathbb{R}^e, \\ f_{pose} : \mathbb{R}^{T \times 24 \times 3} &\rightarrow \mathbb{R}^e \end{aligned}$$

which map the input sequences to embeddings $z_{pc} = f_{pc}(X_{pc})$, $z_{imu} = f_{imu}(X_{imu})$, and $z_{pose} = f_{pose}(X_{pose})$, where $z_{pc}, z_{imu}, z_{pose} \in \mathbb{R}^e$. Furthermore, we work with the setting where a natural language description X_{text} is not provided for each respective

$(X_{pc}, X_{pose}, X_{imu})$ triple. For this reason, the loss for text descriptions is only computed on the subset of the elements in each batch where we have a corresponding quadruple $(X_{pc}, X_{pose}, X_{imu}, X_{text}, tm)$, where $tm \in \mathbb{B}$ represents a boolean mask if there exists a text description X_{text} . In this way, we can effectively ignore the respective elements in the batch B that do not have text descriptions when computing our alignment loss.

Following previous works like CLIP [46], ImageBind [15], MotionCLIP [54], and IMU2CLIP [39], we optimize our encoders using a contrastive objective based on InfoNCE [41]. For a batch of B paired samples, we obtain a boolean mask and embeddings $(z_{pc}^i, z_{imu}^i, z_{pose}^i, z_{text}^i, tm^i)_{i=1}^B$, where z_{text}^i is obtained from a frozen CLIP text encoder. For batch elements i without text pairings, we set tm^i to 0 and use a dummy embedding, tm^i is set to 1 otherwise. The similarity between embeddings is defined using the cosine similarity:

$$\text{sim}(z_a, z_b) = \frac{z_a \cdot z_b}{\|z_a\| \|z_b\|}, \quad (1)$$

where $z_a, z_b \in \{z_{pc}, z_{imu}, z_{pose}, z_{text}\}$. The contrastive loss for each pair (i, j) in the batch is defined as follows:

$$\mathcal{L}_{a \rightarrow b}^i = -\log \frac{\exp(\text{sim}(z_a^i, z_b^i)/\tau)}{\sum_{j=1}^B \exp(\text{sim}(z_a^i, z_b^j)/\tau)} \quad (2)$$

where $a, b \in \{pc, imu, pose, text\}$ and $\tau > 0$ is a (learnable) temperature hyperparameter. Symmetrically, we compute the loss in both directions by swapping the roles of the modalities, i.e., $\mathcal{L}_{a \rightarrow b}^i$ and $\mathcal{L}_{b \rightarrow a}^i$, which leads to:

$$\mathcal{L}_{a,b}^i = \frac{1}{2} (\mathcal{L}_{a \rightarrow b}^i + \mathcal{L}_{b \rightarrow a}^i) \quad (3)$$

As our main goal is to align $z_{pc}, z_{imu}, z_{pose}$, we employ two different losses. First, we bind the subset of paired $z_{pc}, z_{imu}, z_{pose}$ with the respective text embeddings x_{text} :

$$\mathcal{L}_{text}^i = \sum_{i=1}^B tm^i \sum_{a \in M} \mathcal{L}_{a, text}^i \quad (4)$$

where tm^i serves as a mask to ignore the elements in the batch without text pairings for this loss. Second, each individual sensing modality pair $M^* := \{(pc, imu), (pc, pose), (imu, pose)\}$ is optimized to be close to each other:

$$\mathcal{L}_M^i = \sum_{i=1}^B \sum_{(a,b) \in M^*} \mathcal{L}_{a,b}^i \quad (5)$$

In both \mathcal{L}_{text} and \mathcal{L}_M , we do not weight each modality individually. Finally, we combine both losses to enforce aligning embeddings from the corresponding point cloud, IMU, and pose sequences while constraining them to take

small steps toward the text embedding space of CLIP. With $M := \{pc, imu, skeleton\}$ being the set of modalities to align and M^* their respective desired pairings, we optimize the following final loss function for each batch:

$$\mathcal{L}_{total}^i = \alpha \mathcal{L}_{text} + \beta \mathcal{L}_M \quad (6)$$

where $\alpha = 0.5, \beta = 0.5$ equally weight both loss terms.

In our experiments, we train models of all possible modality combinations, which requires an according change to the modality set M and the respective pairings M^* (e.g., training only DeSPE, then $M := \{skeleton, pointcloud\}$). Finally, when training a model like DeSPE without text pairings, the overall loss simplifies to Equation 5, so that $\mathcal{L}_{total}^i = \mathcal{L}_M$.

4. Experiments

We evaluate the effectiveness of DeSPITE and its variants on the following tasks: Modality matching, temporal moment retrieval using a different modality as a query, pre-training for point cloud human activity recognition, and several qualitative evaluations.

4.1. Datasets

We train our method on a merged version of LIPD [48] and Babel [45] (denoted as Babel+LIPD), where we map the text annotations from Babel to the AMASS [36] subsets present in LIPD. In this way, we are able to construct a large-scale dataset of real and synthetic LiDAR point cloud, IMU, and skeleton data with text annotations. To be more specific, we construct two versions of LIPD-Babel. First LIPD-Babel-v1, where we use the official train-test split of LIPD¹, including DIP [21] and TotalCapture (TC) [55]. Second LIPD-Babel-v2, where we use the train-val split of Babel for the AMASS subsets, and add all the remaining data of LIPD to the training set. As LIPD is provided in 10 FPS, we downsample the Babel annotations to 10 FPS. After preprocessing the whole dataset with sliding windows of length 24, we obtain 502,958 / 85,551 training/testing windows for LIPD-Babel-v1, from which 85,551 training windows have text annotations, and 403,430 / 58,802 train/test windows for LIPD-Babel-v2, with 135,699 text training windows and 58,802 test annotations.

Regarding downstream task performance for HAR, we evaluate our approach on HMPEAR [29], MSR-Action3D [27], and our Babel-LIPD-v2 train/test split that only includes Babel sequences. Both HMPEAR and MSR-Action3D include domain shifts, where HMPEAR uses a different kind of LiDAR sensor, and MSR-Action3D has very dense point clouds derived from depth maps.

¹We exclude LidarCap [24] since the data is not available in the official LIPD data repository. More details about LIPD-Babel in Appendix 6.

4.2. Experimental Design and Metrics

We use the following tasks to evaluate the performance of DeSPITE (and its variants) and enable future research to compare against our baselines. Throughout all models in our experiments, all hyperparameters are kept the same.

Task 1. Matching between Modalities

In multi-person scenes, matching IMU data to detected individuals in point cloud sequences is a challenging upstream task, which has not been explored before. This task can be generalized to an any-to-any modality matching problem, which we even further evaluate with this task. We evaluate all modality combinations $\text{IMU} \leftrightarrow \text{PC}$, $\text{IMU} \leftrightarrow \text{Skeleton}$, and $\text{PC} \leftrightarrow \text{Skeleton}$. For each test set (LIPD-Test, TC, DIP), we generate 1000 artificial multi-person scenes (following designs in prior works [37, 40]). This is achieved by randomly sampling n sequences from the test set first and then sampling a respective subsequence, leading to n artificial subjects carrying out an activity simultaneously. The number of subjects per scene varies $n \in (2, 4, 8, 12, 16, 20, 24, 28, 32)$, simulating different real-world scenarios. Given n subjects, we report matching accuracy through argmax on the cosine similarities per row between all candidates.

Task 2. Temporal Moment Retrieval between Modalities

Given a short snippet in one modality, the goal is to retrieve the corresponding temporal moment in the sequence observed with another modality. This task has been explored for, e.g., IMU-RGB [39] and skeleton-text [44], but not yet for LiDAR point clouds, IMU, and skeletons. We evaluate this on the three held-out test sets of LIPD (LIPD-Test, TC, DIP) using $\text{Recall}@k$ ($k = 1, 10, 20, 50$) shots across all modality combinations. Performance is measured by computing the cosine similarity scores for *all* possible query-target pairs in *all* individual test set sequences and returning the top- k similar frame indices. For each query, we compute the difference between all top- k returned time points against the ground truth. A retrieval is considered to be correct if it is within 10 frames ($\sim 1.5\text{sec}$) of the ground truth. As the final score, the mean over all $\text{recall}@k$ scores of all sequences for a dataset is reported.

Task 3. Pre-Training for Human Activity Recognition

We evaluate cross-modal pre-training for point clouds, IMUs, and skeletons via linear/non-linear probing and fine-tuning. HAR pre-training/testing is done on LIPD-Babel-v2, with additional point cloud testing on HMEPAR and MSR-Action3D. Results follow standard metrics: clip segment accuracy for MSR-Action3D, segment accuracy for HMEPAR and LIPD-Babel-v2 (excluding transition labels). We do not evaluate with additional skeleton/IMU datasets, since transfer learning is strongly limited by serious dataset-specific variations in joints and different IMU channel

counts for these modalities.

Task 4. Retrieval between Modalities from Database

We qualitatively evaluate retrieval from a “large database” between Point Cloud \leftrightarrow IMU, IMU \leftrightarrow Skeleton, and Point Cloud \leftrightarrow Skeleton. This enables motion analysis across representations, aiding interpretability (e.g., skeletons or point clouds simplify IMU visualization).

4.3. Implementation Details

For point clouds, we use the PST-Transformer [13] with a SimCLR-based projection head [6]. IMU is encoded with a 2-layer LSTM [19], skeletons with the ACTOR encoder [43], and text with a frozen CLIP text encoder [46]. All models are pre-trained for 145 epochs with 512-d embeddings, Adam optimizer [22], lr=1e-4, batch size 1024. We subsample 256-points using farthest point downsampling (FPD) on each frame and use 24-frame windows as input to all models. Augmentations (random translation, scaling, Gaussian noise) are employed during training to prevent overfitting. For a fair comparison, we only use the weights from epoch 145 across all models. HAR fine-tuning roughly follows [13], with batch size 24, 35 epochs (SGD [49], warmup to lr=0.01, 0.1 decay at epochs 20, 30). In HMEPAR, we subsample 1024 points using FPD and use 24-frame windows. In MSR-Action3D, we follow the standard 2048-point, 24-frame window setting.

4.4. Results: Multi-Person LiDAR-IMU Matching

Figure 2 shows our results for matching between $\text{IMU} \leftrightarrow \text{PC}$, $\text{IMU} \leftrightarrow \text{Skeleton}$, and $\text{PC} \leftrightarrow \text{Skeleton}$ across all trained model variants (all specific numbers in Appendix 7). The subjects are varied on the x-axis, and matching accuracy is reported on the y-axis. Each row corresponds to the respective test set (TC, DIP, LIPD). First, our experiments reveal that models trained with text (i.e., DeSPITE, DePITE, De-SITE, DeSPTE) in almost all scenarios perform worse than models trained solely on the modalities alone (i.e., DeSPE, DePIE, DeSIE, DESPIE), showing that this task does not benefit from text embeddings. Second, we find that matching between IMU, point clouds, and skeletons can be effectively learned, showing up to perfect matching scores for a smaller number of subjects. In comparison, a larger number of subjects, as expected, becomes more challenging.

4.5. Results: Temporal Moment Retrieval

Figure 3 shows our results for temporal moment retrieval between $\text{IMU} \leftrightarrow \text{Pointcloud}$, $\text{IMU} \leftrightarrow \text{Skeleton}$, and $\text{Pointcloud} \leftrightarrow \text{Skeleton}$ across all trained model variants (all specific numbers in Appendix 7). The k retrieval shots are varied on the x-axis, and the respective $\text{recall}@k$ is reported on the y-axis. Each row shows the results for each respective test set (TC, DIP, LIPD). First, we observe the same

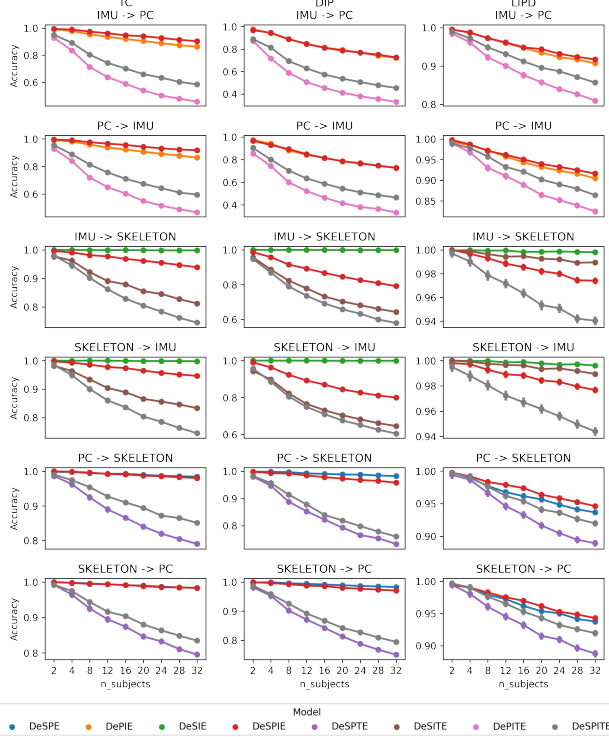


Figure 2. Matching performance between all modality pairs $\text{IMU} \leftrightarrow \text{Pointcloud}$, $\text{IMU} \leftrightarrow \text{Skeleton}$, $\text{Pointcloud} \leftrightarrow \text{Skeleton}$, reporting mean accuracy for $n \in \{2, 4, 8, 12, 16, 20, 24, 28, 32\}$ subjects across 1000 artificial scenes.

result for temporal moment retrieval as for matching in Figure 2: All models trained with text perform worse than models trained solely on the modalities alone. Second, our evaluation demonstrates that temporal moment retrieval can be solved the best between $\text{IMU} \leftrightarrow \text{Skeleton}$, where DeSIE demonstrates that training between both modalities alone is very effective. The runner-up is $\text{Pointcloud} \leftrightarrow \text{Skeleton}$ where DeSPIE and DeSPE achieve almost identical performance. Finally, our experiments reveal that the most challenging problem is $\text{IMU} \leftrightarrow \text{Point cloud}$ matching, allowing future work to propose more effective solutions.

4.6. Results: 3D Point Cloud Human Activity Recognition

The pre-trained embeddings of all versions of DeSPITE can be fine-tuned for HAR. We compare our approach against the recent state-of-the-art on MSR-Action3D, HMPEAR, and perform ablations on the LIPD-Babel-v2 split.

MSR-Action3D: Table 1 shows that fine-tuning DeSPITE, DeSPIE, or DePITE embeddings surpasses *all* current state-of-the-art point cloud HAR pre-training methods, despite encountering a domain shift from 256 to 2048 points. Our approach, combined with PST-Transformer, even outperforms PvNext [59] (94.77<95.47)

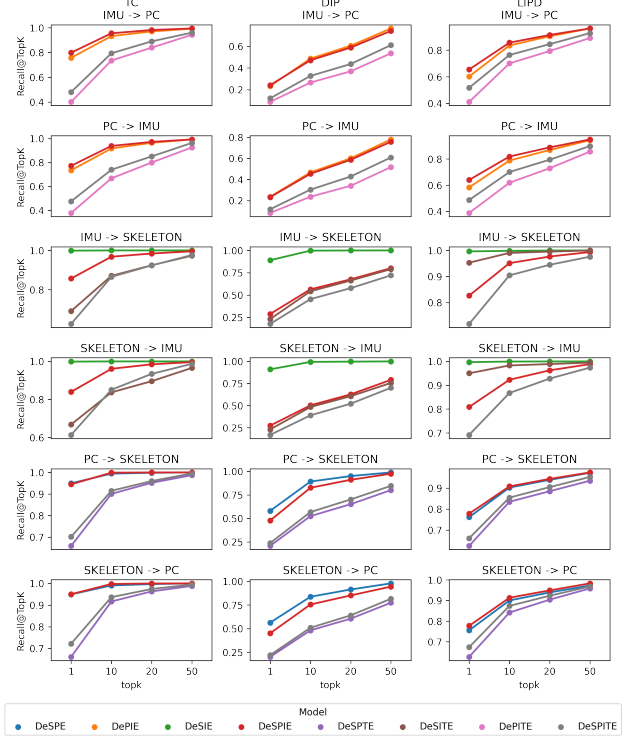


Figure 3. Temporal moment retrieval performance across all modalities. Recall is reported for top-1, 10, 20, and 50 retrievals, considering a match correct if within 10 frames of the ground truth (\approx half the window size).

and MAMBA4D [31] (93.38<95.47) and nearly matches KAN-HyperpointNet [7] (95.59>95.47).

HMPEAR: As shown in Table 2, we achieve new SOTA on HMPEAR, outperforming all prior point cloud, RGB, and multi-modal approaches. While our setup uses twice the frames of previous methods, pretraining PST-Transformer in the same setup with DeSPITE, DeSPIE, or DePITE improves its performance by nearly 4%, demonstrating the effectiveness for HAR pre-training.

LIPD-Babel-v2: Table 3 shows that all our models outperform baselines (PST-Transformer, LSTM, ACTOR) when trained from scratch on LIPD-Babel-v2. We explore various freezing strategies, as well as linear/non-linear probing and projection heads, with detailed ablations in the supplementary material (Tables 6,7,8). In Table 3, only the best results of DePITE, DeSPIE, and DeSPITE are reported, which consistently achieve strong performance across all three datasets.

Notably, across MSR-Action3D and HMPEAR, DeSPITE, DeSPIE, and DePITE consistently achieve the best performance, underlining the advantage of pre-training with more modalities. Furthermore, different from the results for matching and temporal moment retrieval, we find that training with text benefits the fine-tuning performance for HAR.

Methods	Video Acc@1 (\uparrow)
<i>Supervised Learning Only</i>	
MeteorNet [32]	88.50
PSTNet [11]	91.20
P4Transformer [10]	90.94
Kinet [65]	93.27
PPTr [60]	92.33
PSTNet++ [12]	92.68
Leaf [33]	93.84
PST-Transformer [13]	93.73
PST-Transformer [†] [13]	92.33
MAMBA4D [31]	93.38
PvNext [59]	94.77
KAN-HyperpointNet [7]	95.59
<i>Uni-Modal Pre-Training + Transfer Learning</i>	
PSTNet + PointCPSC [53]	92.68 (+1.48)
PSTNet + PointCMP [52]	93.27 (+2.07)
PST-Transformer + MaST-Pre [51]	94.08 (+0.35)
PPTr + C2P [64]	94.76 (+2.43)
P4Transformer + M2PSC [18]	93.03 (+2.09)
PST-Transformer + M2PSC [18]	94.84 (+1.11)
<i>Multi-Modal Pre-Training + Transfer Learning</i>	
PST-Transformer + DePITE (Ours)	95.12 (+1.39 + 2.79 [†])
PST-Transformer + DeSPIE (Ours)	95.47 (+1.74 + 3.14 [†])
PST-Transformer + DeSPITE (Ours)	95.47 (+1.74 + 3.14 [†])

Table 1. 24-frame classification results on the MSR-Action3D dataset, clip-level accuracy (Acc) is reported.

Method	Modality	Acc(Seg) \uparrow
<i>Uni-Modal Supervised Learning Only</i>		
PSTNet [11]	PC	64.3
P4-Transformer [10]	PC	63.9
PST-Transformer [†] [13]	PC	65.94
I3D [5]	RGB	55.5
SlowFast [14]	RGB	62.2
TimeSformer [3]	RGB	56.3
Uniformer [25]	RGB	61.6
<i>Multi-Modal Supervised Learning Only</i>		
AR-Proj [29]	RGB+PC	60.6
PEAR-Proj (BestPE) [29]	RGB+PC	64.1
PEAR-Proj (BestAR) [29]	RGB+PC	66.0
<i>Multi-Modal Pre-Training + Transfer Learning</i>		
PST-Transformer + DeSPITE (ours)	PC	69.18 (+3.24)
PST-Transformer + DeSPIE (ours)	PC	70.26 (+4.32)
PST-Transformer + DePITE (ours)	PC	70.65 (+4.71)

Table 2. HAR classification results on the HMPEAR action recognition dataset, segment-level accuracy Acc(Seg) is reported.

4.7. Qualitative Results: Embedding Space

Using TSNE [56], we analyze the learned embedding space of DeSPITE and DeSPIE. Figure 4 (a, b) shows embeddings of the same 50-frame sequence per modality (skeletons \bullet , point clouds \times , IMU \star), where both models exhibit strong cross-modal alignment, although DeSPIE demonstrates tighter associations. Figure 4 (c, d) extends this to 20 sequences, revealing distinct clusters that indicate semantic motion encoding. However, DeSPIE’s embeddings are more distinct, qualitatively supporting our retrieval findings and confirming that text embeddings negatively affect matching and temporal moment retrieval performance.

Method	Modality	Acc(Seg) \uparrow
<i>Uni-Modal Supervised Baselines</i>		
PST-Transformer [†] [13]	PC	67.38
LSTM [†] [19]	IMU	65.62
ACTOR [†] [43]	Skeleton	68.23
<i>w/ Zero Shot</i>		
PST-Transformer	PC	30.42
LSTM	IMU	29.88
ACTOR	Skeleton	34.89
<i>w/ Linear Probing</i>		
PST-Transformer	PC	67.06
LSTM	IMU	58.29
ACTOR	Skeleton	61.76
PST-Transformer	PC	67.06
LSTM	IMU	62.06
ACTOR	Skeleton	67.20
<i>w/ Finetuning</i>		
PST-Transformer	PC	67.51
LSTM	IMU	69.21 (+3.59)
ACTOR	Skeleton	68.31
PST-Transformer	PC	69.00 (+1.62)
LSTM	IMU	68.40
ACTOR	Skeleton	70.64 (+2.41)

Table 3. HAR classification results on the Babel-LIPD-v2-CLS action recognition dataset, segment-level accuracy Acc(Seg) is reported.

4.8. Qualitative Results: Retrieval from AMASS and LIPD Database

Figure 5 shows that we can interpret IMU signals using our method by querying a large motion database like AMASS or LIPD. We show retrievals of skeletons from AMASS and point clouds from LIPD using IMU (top) as a query, also showing the ground truth. The retrievals semantically capture the motion performed by the IMU signal, allowing us to understand that the IMU signal corresponds to walking while turning (left), doing a lunge (middle), and forward stretch (right), respectively. Extending IMU2CLIP [39], our method can help interpret IMU signals with skeletons and point cloud sequences.

Figure 6 shows the corresponding retrievals between skeleton and point clouds. On the left, a pedestrian performs a “lunge” motion, captured effectively by the retrieved skeletons from the AMASS database. On the right, a pedestrian performs a t-pose and then moves his arm into a normal standing position. The retrieved point clouds from the LIPD database follow these motions, showing a learned correspondence of motion between both modalities. We can see that different motion sequences are retrieved with different point cloud densities. *To better assess the effectiveness of DeSPITE for cross-modal retrieval*, we provide animated videos in the supplementary material.

4.9. Qualitative Results: Temporal Moment Retrieval

Figure 7 illustrates how effectively an encoded IMU query can retrieve relevant moments in a point cloud video. We

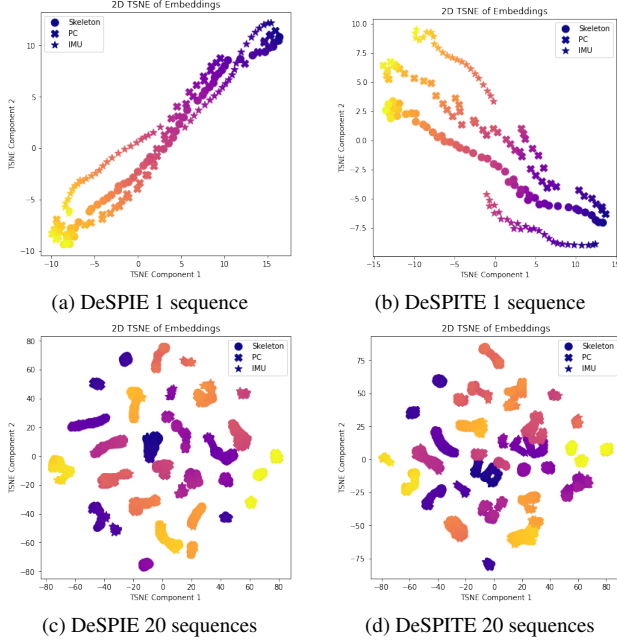


Figure 4. Using TSNE, we visualize the joint embedding space between skeletons (●), point clouds (×), and IMU (★) on 1 (a,b) and 20 (c,d) randomly sampled sequences with 50 consecutive sequences of both DeSPIE (left) and DeSPITE (right). Each point is colored by its time index with a colormap to emphasize the similarity among each of the modalities over time.

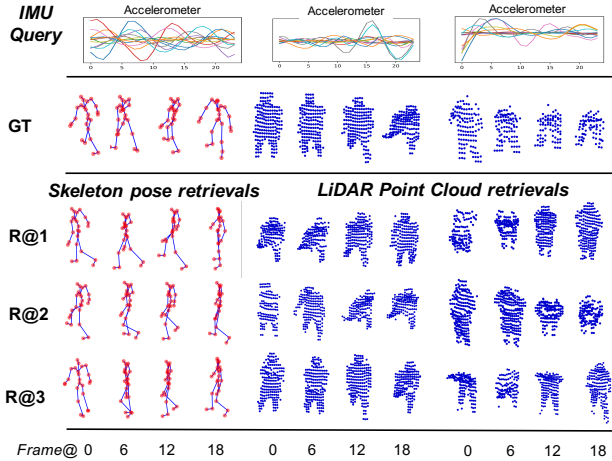


Figure 5. IMU→Skeleton and IMU→Point cloud Retrieval from AMASS and LIPD database, respectively.

visualize cosine similarity across a 1400-frame sequence containing diverse activities, with peaks aligning precisely with the ground truth timestamps. Despite no explicit training for this, in Query 2, our approach identifies repeated instances of a person standing still, highlighting the ability of DeSPITE to encode semantic meaning for certain ac-

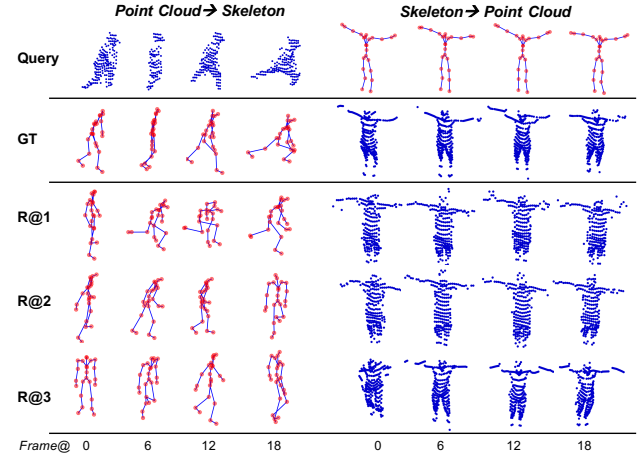


Figure 6. Point cloud→Skeleton and Skeleton→Point cloud Retrieval from AMASS and LIPD database, respectively.

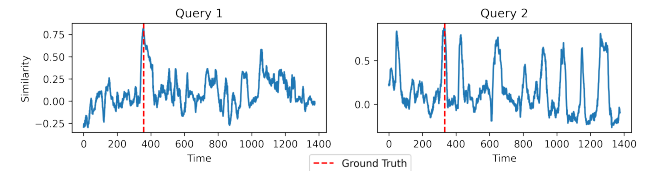


Figure 7. We show two random IMU queries to localize the respective moment in a 1400 frame-long point cloud sequence from the unseen LIPD test.

ivities within the embedding space. **We provide an animated video** of this in the supplementary material (“temporal_moment_retrieval/temporal_retrieval_imu.gif”).

5. Conclusion

We introduce DeSPITE, a **Deep Skeleton-Pointcloud-IMU-Text Embedding** model, enabling novel cross-modal tasks such as matching for re-identification, temporal moment retrieval, and retrieval across modalities. Unlike prior RGB-centric approaches, DeSPITE leverages LiDAR point clouds as the primary visual modality for contrastive learning. On the constructed LIPD-Babel dataset, we establish strong baselines for these tasks, providing a foundation for future comparisons. Additionally, we demonstrate that contrastive pre-training for HAR with DeSPITE achieves new state-of-the-art performance on MSR-Action3D and HMP-EAR. Our findings highlight that text-enhanced embeddings benefit HAR but slightly limit retrieval performance compared to text-free variants. This work paves the way for general-purpose LiDAR-based video encoders for human activity understanding.

References

[1] Matteo Bastico, Verónica Ruiz Bejerano, and Alberto Belmonte-Hernández. Simultaneous real-time human fall detection and reidentification based on multisensors data. In *Proceedings of the 15th International Conference on PErvasive Technologies Related to Assistive Environments*, pages 365–370, 2022. 1, 3

[2] Léore Bensabath, Mathis Petrovich, and Gul Varol. A cross-dataset study for text-based 3d human motion retrieval. In *Proceedings of the IEEE/CVF Conference on Computer Vision and Pattern Recognition*, pages 1932–1940, 2024. 2

[3] Gedas Bertasius, Heng Wang, and Lorenzo Torresani. Is space-time attention all you need for video understanding? In *ICML*, page 4, 2021. 7

[4] Bryan Bo Cao, Abrar Alali, Hansi Liu, Nicholas Meegan, Marco Gruteser, Kristin Dana, Ashwin Ashok, and Shubham Jain. Vitag: Online wifi fine time measurements aided vision-motion identity association in multi-person environments. In *2022 19th Annual IEEE International Conference on Sensing, Communication, and Networking (SECON)*, pages 19–27. IEEE, 2022. 1, 3

[5] Joao Carreira and Andrew Zisserman. Quo vadis, action recognition? a new model and the kinetics dataset. In *proceedings of the IEEE Conference on Computer Vision and Pattern Recognition*, pages 6299–6308, 2017. 7

[6] Ting Chen, Simon Kornblith, Mohammad Norouzi, and Geoffrey Hinton. A simple framework for contrastive learning of visual representations. In *International conference on machine learning*, pages 1597–1607. PMLR, 2020. 5

[7] Zhaoyu Chen, Xing Li, Qian Huang, Qiang Geng, Tianjin Yang, and Shihao Han. Kan-hyperpointnet for point cloud sequence-based 3d human action recognition. *arXiv preprint arXiv:2409.09444*, 2024. 6, 7

[8] Shenghong Dai, Shiqi Jiang, Yifan Yang, Ting Cao, Mo Li, Suman Banerjee, and Lili Qiu. Advancing multi-modal sensing through expandable modality alignment. *arXiv preprint arXiv:2407.17777*, 2024. 1, 2, 3

[9] Jacob Devlin, Ming-Wei Chang, Kenton Lee, and Kristina Toutanova. Bert: Pre-training of deep bidirectional transformers for language understanding. In *Proceedings of the 2019 conference of the North American chapter of the association for computational linguistics: human language technologies, volume 1 (long and short papers)*, pages 4171–4186, 2019. 2

[10] Hehe Fan, Yi Yang, and Mohan Kankanhalli. Point 4d transformer networks for spatio-temporal modeling in point cloud videos. In *Proceedings of the IEEE/CVF conference on computer vision and pattern recognition*, pages 14204–14213, 2021. 7

[11] Hehe Fan, Xin Yu, Yuhang Ding, Yi Yang, and Mohan Kankanhalli. Pstnet: Point spatio-temporal convolution on point cloud sequences. In *International Conference on Learning Representations*, 2021. 7

[12] Hehe Fan, Xin Yu, Yi Yang, and Mohan Kankanhalli. Deep hierarchical representation of point cloud videos via spatio-temporal decomposition. *IEEE Transactions on Pattern Analysis and Machine Intelligence*, 44(12):9918–9930, 2021. 7

[13] Hehe Fan, Yi Yang, and Mohan Kankanhalli. Point spatio-temporal transformer networks for point cloud video modeling. *IEEE Transactions on Pattern Analysis and Machine Intelligence*, 45(2):2181–2192, 2022. 5, 7

[14] Christoph Feichtenhofer, Haoqi Fan, Jitendra Malik, and Kaiming He. Slowfast networks for video recognition. In *Proceedings of the IEEE/CVF international conference on computer vision*, pages 6202–6211, 2019. 7

[15] Rohit Girdhar, Alaaeldin El-Nouby, Zhuang Liu, Mannat Singh, Kalyan Vasudev Alwala, Armand Joulin, and Ishan Misra. Imagebind: One embedding space to bind them all. In *Proceedings of the IEEE/CVF conference on computer vision and pattern recognition*, pages 15180–15190, 2023. 1, 2, 3, 4

[16] Chuan Guo, Shihao Zou, Xinxin Zuo, Sen Wang, Wei Ji, Xingyu Li, and Li Cheng. Generating diverse and natural 3d human motions from text. In *Proceedings of the IEEE/CVF Conference on Computer Vision and Pattern Recognition (CVPR)*, pages 5152–5161, 2022. 3

[17] Mark Hamilton, Andrew Zisserman, John R Hershey, and William T Freeman. Separating the “chirp” from the “chat”: Self-supervised visual grounding of sound and language. In *Proceedings of the IEEE/CVF conference on computer vision and pattern recognition*, pages 13117–13127, 2024. 3

[18] Yuehui Han, Can Xu, Rui Xu, Jianjun Qian, and Jin Xie. Masked motion prediction with semantic contrast for point cloud sequence learning. In *European Conference on Computer Vision*, pages 414–431. Springer, 2024. 3, 7

[19] Sepp Hochreiter and Jürgen Schmidhuber. Long short-term memory. *Neural computation*, 9(8):1735–1780, 1997. 5, 7

[20] Gang Huang, Zhaozheng Hu, Jie Wu, Hanbiao Xiao, and Fan Zhang. Wifi and vision-integrated fingerprint for smartphone-based self-localization in public indoor scenes. *IEEE Internet of Things Journal*, 7(8):6748–6761, 2020. 1

[21] Yinghao Huang, Manuel Kaufmann, Emre Aksan, Michael J Black, Otmar Hilliges, and Gerard Pons-Moll. Deep inertial poser: Learning to reconstruct human pose from sparse inertial measurements in real time. *ACM Transactions on Graphics (TOG)*, 37(6):1–15, 2018. 4, 1

[22] Diederik P Kingma and Jimmy Ba. Adam: A method for stochastic optimization. *arXiv preprint arXiv:1412.6980*, 2014. 5

[23] Bruno Korbar, Du Tran, and Lorenzo Torresani. Cooperative learning of audio and video models from self-supervised synchronization. *Advances in Neural Information Processing Systems*, 31, 2018. 3

[24] Jialian Li, Jingyi Zhang, Zhiyong Wang, Siqi Shen, Chenglu Wen, Yuexin Ma, Lan Xu, Jingyi Yu, and Cheng Wang. Liddarcap: Long-range marker-less 3d human motion capture with lidar point clouds. In *Proceedings of the IEEE/CVF conference on computer vision and pattern recognition*, pages 20502–20512, 2022. 1, 3, 4

[25] Kunchang Li, Yali Wang, Peng Gao, Guanglu Song, Yu Liu, Hongsheng Li, and Yu Qiao. Uniformer: Unified transformer for efficient spatiotemporal representation learning. *arXiv preprint arXiv:2201.04676*, 2022. 7

[26] Ruilong Li, Shan Yang, David A Ross, and Angjoo Kanazawa. Ai choreographer: Music conditioned 3d dance generation with aist++. In *Proceedings of the IEEE/CVF international conference on computer vision*, pages 13401–13412, 2021. 1

[27] Wanqing Li, Zhengyou Zhang, and Zicheng Liu. Action recognition based on a bag of 3d points. In *2010 IEEE computer society conference on computer vision and pattern recognition-workshops*, pages 9–14. IEEE, 2010. 2, 3, 4

[28] Jia-Ming Liang, Shashank Mishra, and Chun-Che Wu. Enhancing person identification for smart cities: Fusion of video surveillance and wearable device data based on machine learning. *IEEE Sensors Journal*, 2024. 3

[29] Yitai Lin, Zhijie Wei, Wanfa Zhang, Xiping Lin, Yudi Dai, Chenglu Wen, Siqi Shen, Lan Xu, and Cheng Wang. Hmpear: A dataset for human pose estimation and action recognition. In *Proceedings of the 32nd ACM International Conference on Multimedia*, pages 2069–2078, 2024. 1, 2, 3, 4, 7

[30] Jun Liu, Amir Shahroudy, Mauricio Perez, Gang Wang, Ling-Yu Duan, and Alex C Kot. Ntu rgb+d 120: A large-scale benchmark for 3d human activity understanding. *IEEE Transactions on Pattern Analysis and Machine Intelligence*, 42(10):2684–2701, 2020. 3

[31] Jiuming Liu, Jinru Han, Lihao Liu, Angelica I Aviles-Rivero, Chaokang Jiang, Zhe Liu, and Hesheng Wang. Mamba4d: Efficient long-sequence point cloud video understanding with disentangled spatial-temporal state space models. *arXiv preprint arXiv:2405.14338*, 2024. 6, 7

[32] Xingyu Liu, Mengyuan Yan, and Jeannette Bohg. Meteor-net: Deep learning on dynamic 3d point cloud sequences. In *Proceedings of the IEEE/CVF International Conference on Computer Vision*, pages 9246–9255, 2019. 7

[33] Yunze Liu, Junyu Chen, Zekai Zhang, Jingwei Huang, and Li Yi. Leaf: Learning frames for 4d point cloud sequence understanding. In *Proceedings of the IEEE/CVF International Conference on Computer Vision*, pages 604–613, 2023. 7

[34] Matthew Loper, Naureen Mahmood, Javier Romero, Gerard Pons-Moll, and Michael J Black. Smpl: A skinned multi-person linear model. In *Seminal Graphics Papers: Pushing the Boundaries, Volume 2*, pages 851–866. 2023. 1

[35] Mingqi Lu, Siyuan Yang, Xiaobo Lu, and Jun Liu. Cross-modal contrastive pre-training for few-shot skeleton action recognition. *IEEE Transactions on Circuits and Systems for Video Technology*, 2024. 3

[36] Naureen Mahmood, Nima Ghorbani, Nikolaus F. Troje, Gerard Pons-Moll, and Michael J. Black. AMASS: Archive of motion capture as surface shapes. In *International Conference on Computer Vision*, pages 5442–5451, 2019. 3, 4, 1

[37] Alessandro Masullo, Tilo Burghardt, Dima Damen, Toby Perrett, and Majid Mirmehdi. Who goes there? exploiting silhouettes and wearable signals for subject identification in multi-person environments. In *Proceedings of the IEEE/CVF International Conference on Computer Vision Workshops*, pages 0–0, 2019. 1, 3, 5

[38] Alessandro Masullo, Tilo Burghardt, Dima Damen, Toby Perrett, and Majid Mirmehdi. Person re-id by fusion of video silhouettes and wearable signals for home monitoring applications. *Sensors*, 20(9):2576, 2020. 1, 3

[39] Seungwhan Moon, Andrea Madotto, Zhaojiang Lin, Aparajita Saraf, Amy Bearman, and Babak Damavandi. Imu2clip: Language-grounded motion sensor translation with multi-modal contrastive learning. In *Findings of the Association for Computational Linguistics: EMNLP 2023*, pages 13246–13253, 2023. 1, 2, 3, 4, 5, 7

[40] Alisher Mukashev, Lan-Da Van, Susanta Sharma, M Farhan Tandia, and Yu-Chee Tseng. Person tracking by fusing posture data from uav video and wearable sensors. *IEEE Sensors Journal*, 22(24):24150–24160, 2022. 5

[41] Aaron van den Oord, Yazhe Li, and Oriol Vinyals. Representation learning with contrastive predictive coding. *arXiv preprint arXiv:1807.03748*, 2018. 1, 3, 4

[42] Maxime Oquab, Timothée Darcet, Théo Moutakanni, Huy Vo, Marc Szafraniec, Vasil Khalidov, Pierre Fernandez, Daniel Haziza, Francisco Massa, Alaaddin El-Nouby, et al. Dinov2: Learning robust visual features without supervision. *arXiv preprint arXiv:2304.07193*, 2023. 2

[43] Mathis Petrovich, Michael J Black, and GÜl Varol. Action-conditioned 3d human motion synthesis with transformer vae. In *Proceedings of the IEEE/CVF International Conference on Computer Vision*, pages 10985–10995, 2021. 5, 7

[44] Mathis Petrovich, Michael J Black, and GÜl Varol. Tmr: Text-to-motion retrieval using contrastive 3d human motion synthesis. In *Proceedings of the IEEE/CVF International Conference on Computer Vision*, pages 9488–9497, 2023. 3, 5

[45] Abhinanda R. Punnakkal, Arjun Chandrasekaran, Nikos Athanasiou, Alejandra Quiros-Ramirez, and Michael J. Black. BABEL: Bodies, action and behavior with english labels. In *Proceedings IEEE/CVF Conf. on Computer Vision and Pattern Recognition (CVPR)*, pages 722–731, 2021. 2, 3, 4, 1

[46] Alec Radford, Jong Wook Kim, Chris Hallacy, Aditya Ramesh, Gabriel Goh, Sandhini Agarwal, Girish Sastry, Amanda Askell, Pamela Mishkin, Jack Clark, et al. Learning transferable visual models from natural language supervision. In *International conference on machine learning*, pages 8748–8763. PMLR, 2021. 1, 2, 4, 5

[47] Nikhila Ravi, Valentin Gabeur, Yuan-Ting Hu, Ronghang Hu, Chaitanya Ryali, Tengyu Ma, Haitham Khedr, Roman Rädle, Chloe Rolland, Laura Gustafson, Eric Mintun, Junting Pan, Kalyan Vasudev Alwala, Nicolas Carion, Chao-Yuan Wu, Ross Girshick, Piotr Dollár, and Christoph Feichtenhofer. Sam 2: Segment anything in images and videos. *arXiv preprint arXiv:2408.00714*, 2024. 2

[48] Yiming Ren, Chengfeng Zhao, Yannan He, Peishan Cong, Han Liang, Jingyi Yu, Lan Xu, and Yuexin Ma. Lidar-aid inertial poser: Large-scale human motion capture by sparse inertial and lidar sensors. *IEEE Transactions on Visualization and Computer Graphics*, 29(5):2337–2347, 2023. 1, 2, 3, 4

[49] Sebastian Ruder. An overview of gradient descent optimization algorithms. *arXiv preprint arXiv:1609.04747*, 2016. 5

[50] Amir Shahroudy, Jun Liu, Tian-Tsong Ng, and Gang Wang. Ntu rgb+d: A large scale dataset for 3d human activity analysis. In *Proceedings of the IEEE conference on computer vision and pattern recognition*, pages 1010–1019, 2016. 3

[51] Zhiqiang Shen, Xiaoxiao Sheng, Hehe Fan, Longguang Wang, Yulan Guo, Qiong Liu, Hao Wen, and Xi Zhou. Masked spatio-temporal structure prediction for self-supervised learning on point cloud videos. In *Proceedings of the IEEE/CVF International Conference on Computer Vision*, pages 16580–16589, 2023. 3, 7

[52] Zhiqiang Shen, Xiaoxiao Sheng, Longguang Wang, Yulan Guo, Qiong Liu, and Xi Zhou. Pointcmp: Contrastive mask prediction for self-supervised learning on point cloud videos. In *Proceedings of the IEEE/CVF Conference on Computer Vision and Pattern Recognition*, pages 1212–1222, 2023. 3, 7

[53] Xiaoxiao Sheng, Zhiqiang Shen, Gang Xiao, Longguang Wang, Yulan Guo, and Hehe Fan. Point contrastive prediction with semantic clustering for self-supervised learning on point cloud videos. In *Proceedings of the IEEE/CVF International Conference on Computer Vision*, pages 16515–16524, 2023. 3, 7

[54] Guy Tevet, Brian Gordon, Amir Hertz, Amit H Bermano, and Daniel Cohen-Or. Motionclip: Exposing human motion generation to clip space. In *European Conference on Computer Vision*, pages 358–374. Springer, 2022. 1, 2, 3, 4

[55] Matthew Trumble, Andrew Gilbert, Charles Malleson, Adrian Hilton, and John Collomosse. Total capture: 3d human pose estimation fusing video and inertial sensors. In *Proceedings of 28th British Machine Vision Conference*, pages 1–13, 2017. 4, 1

[56] Laurens Van der Maaten and Geoffrey Hinton. Visualizing data using t-sne. *Journal of machine learning research*, 9(11), 2008. 7

[57] Timo von Marcard, Roberto Henschel, Michael Black, Bodo Rosenhahn, and Gerard Pons-Moll. Recovering accurate 3d human pose in the wild using imus and a moving camera. In *European Conference on Computer Vision (ECCV)*, 2018. 1, 3

[58] Haiyan Wang, Liang Yang, Xuejian Rong, Jinglun Feng, and Yingli Tian. Self-supervised 4d spatio-temporal feature learning via order prediction of sequential point cloud clips. In *Proceedings of the IEEE/CVF Winter Conference on Applications of Computer Vision*, pages 3762–3771, 2021. 3

[59] Jie Wang, Tingfa Xu, Lihe Ding, Xinjie Zhang, Long Bai, and Jianan Li. Pvnext: Rethinking network design and temporal motion for point cloud video recognition. In *The Thirteenth International Conference on Learning Representations*. 6, 7

[60] Hao Wen, Yunze Liu, Jingwei Huang, Bo Duan, and Li Yi. Point primitive transformer for long-term 4d point cloud video understanding. In *European Conference on Computer Vision*, pages 19–35. Springer, 2022. 7

[61] Yiteng Xu, Peishan Cong, Yichen Yao, Runnan Chen, Yuenan Hou, Xinge Zhu, Xuming He, Jingyi Yu, and Yuexin Ma. Human-centric scene understanding for 3d large-scale scenarios. In *Proceedings of the IEEE/CVF International Conference on Computer Vision*, pages 20349–20359, 2023. 1, 3

[62] Jianfei Yang, He Huang, Yunjiao Zhou, Xinyan Chen, Yuecong Xu, Shanghai Yuan, Han Zou, Chris Xiaoxuan Lu, and Lihua Xie. Mm-fi: Multi-modal non-intrusive 4d human dataset for versatile wireless sensing. *Advances in Neural Information Processing Systems*, 36:18756–18768, 2023. 3

[63] Kangning Yin, Shihao Zou, Yuxuan Ge, and Zheng Tian. Tri-modal motion retrieval by learning a joint embedding space. In *Proceedings of the IEEE/CVF Conference on Computer Vision and Pattern Recognition*, pages 1596–1605, 2024. 1, 2, 3

[64] Zhuoyang Zhang, Yuhao Dong, Yunze Liu, and Li Yi. Complete-to-partial 4d distillation for self-supervised point cloud sequence representation learning. In *Proceedings of the IEEE/CVF conference on computer vision and pattern recognition*, pages 17661–17670, 2023. 3, 7

[65] Jia-Xing Zhong, Kaichen Zhou, Qingyong Hu, Bing Wang, Niki Trigoni, and Andrew Markham. No pain, big gain: classify dynamic point cloud sequences with static models by fitting feature-level space-time surfaces. In *Proceedings of the IEEE/CVF Conference on Computer Vision and Pattern Recognition*, pages 8510–8520, 2022. 7

DeSPITE: Exploring Contrastive Deep Skeleton-Pointcloud-IMU-Text Embeddings for Advanced Point Cloud Human Activity Understanding

Supplementary Material

	LIPD-Babel-v1	LIPD-Babel-v2
#Sequences Train	502958	403430
#Sequences Test	85551	58802
#Text Train	187641	135699
#Text Test	-	58802

Table 4. Number of total training sequences and frame-wise text labels when considering 24 frame sequences at 10 fps in LIPD-Babel-v1 and LIPD-Babel-v2.

6. More Information on LIPD-Babel

LIPD [48] is a large-scale dataset combining LiDAR point clouds, IMU, and skeleton poses. It includes a mix of real and synthetic LiDAR point clouds and IMU measurements, taking advantage of the AMASS [36] motion capture dataset. It combines their own recorded real sequences with ground truth SMPL [34] pose parameters from DIP-IMU [21], LiDARHuman26M [48], AIST++[26], and a subset of AMASS [36] (including ACCAD, BML-Movi, CMU, and TotalCapture(TC) [55]). From this large collection of data, DIP-IMU, TC, the testing set of LiDARHuman26M, and their LIPD test set are used for evaluation, while the remaining data is used as the training set. From the SMPL poses of the AMASS subsets and AIST++, LIPD has generated synthetic point clouds and IMU recordings. For DIP-IMU, they generated synthetic point clouds, and took the real IMU recordings. For LiDARHuman26M, real point clouds are provided, and LIPD generated synthetic IMU recordings. LIPD has provided more details on the generation in the supplementary material of their work but did not publish the code.

While LIPD is a large-scale data for human motion with LiDAR, IMU, and skeletal poses, it is missing activity annotations. Fortunately, the Babel dataset [45] has annotated the AMASS dataset with strong efforts with frame-wise activity annotations. Taking advantage of these annotations, we have merged the Babel annotations into the corresponding AMASS subsets present in LIPD, i.e., ACCAD, BML-Movi, CMU, and TC.

To achieve this, we take advantage of the specific sequence ID’s for each AMASS sequence that are stored both in LIPD and in Babel. This allows a unique mapping between both datasets, allowing to add text annotations to the AMASS subset in LIPD. More specifically, all AMASS sequence ids follow the pattern of

“dataset/sequencecategory/posessequence_poses.npz”. For example, “ACCAD/Female1Gestures_c3d/D2_-Wait_1_poses.npz” or “CMU/118/118.17_poses.npz”. In LIPD, these sequence ids were modified to follow the pattern “dataset/sequencecategory/posessequence_stageii”, leading to “ACCAD/Female1Gestures_c3d/D2_-Wait_1_stageii” “CMU/118/118_17_stageii”. Therefore, to achieve the mapping, a reformatting is required by replacing “stageii” with “poses.npz”. Babel follows the exact same format as AMASS, allowing a straightforward mapping from the AMASS subset in LIPD to the respective subset in Babel.

The next difference is the sampling rate of the dataset. AMASS is provided at a higher FPS up to 120FPS, which is much higher than the 10 FPS of LIPD, while Babel is annotated at 30FPS. As a result, we downsample the Babel annotations accordingly to 10FPS to align them with the LIPD dataset. To verify that both datasets are actually temporally aligned after downsampling Babel to 10 FPS, we carefully verified qualitatively that the skeleton poses of the downsampled Babel versions correspond to the poses in the LIPD dataset by plotting them next to each other, and inspecting several sequences from each dataset manually.

When combining Babel and LIPD to LIPD-Babel, we obtain two versions of the dataset. First, LIPD-Babel-v1, which follows the exact test split of LIPD, and LIPD-Babel-v2, which follows the train/val/test split of Babel. LIPD-Babel-v1 allows to evaluate the respective matching and retrieval tasks, while LIPD-Babel-v2 allows to evaluate classification tasks with labels for both training and testing set. More specifically, for LIPD-Babel-v2, the official training split of Babel is used for the training set, and the validation split for the testing set. The annotations for the test split are not publicly available, which is why we use the validation set as the testing set replacement.

Finally, we preprocess the whole dataset into 24-frame sliding window subsequences to ease the training and testing process. A summary of the number of sequences and corresponding text annotations are provided in Table 4. LIPD-Babel-v1 has slightly more sequences than LIPD-Babel-v2 because the test set of Babel is not publicly available, because of which we remove the sequences from ACCAD, BML-movi, CMU, and TC that do not have annotations.

7. Specific Performance Scores for Matching and Temporal Moment Retrieval

Figure 2 and Figure 3 in the main paper effectively visualizes the differences in the performance of each model and parameters for matching and temporal moment retrieval, which makes a comparison at the scale of the amount of different parameters that we have evaluated easier to see.

In this section of our supplementary material, we provide the specific matching scores between each modality and each dataset through a heatmap in Figure 8 to provide quantitative numbers for future work to compare against our baselines. In the same way, we present the specific temporal moment retrieval scores between each modality and each dataset through a heatmap in Figure 9. These results are the average over the number of subjects for matching and k-shots for temporal moment retrieval. All individual results for each number of subjects for matching, and top-k for temporal moment retrieval are provided in Figures 11-18, and Figures 19-22, respectively.

8. A Simple Improved Matching Algorithm to Associate Different Modalities in the Embedding Space

In practice, we observe continuous streams of point cloud, skeleton, and IMU time series data. Therefore, a matching score can be computed not only on similarities between a single query sequence and all possible subsequences of a video, but instead on consecutive subsequences. We define such a matching algorithm in Algorithm 1, where the mean similarity score over several embeddings from a short temporal neighborhood is considered to compute the temporal matching score. More specifically, given N consecutive subsequences with their respective Q consecutive query embeddings $Z_{a,q}^j$, $q \in Q$ from modality a and K consecutive candidate embeddings $Z_{b,k}^j$, $k \in K$ for modality b , $j \leq 0 < N$. The similarity score between each query $q \in Q$ and candidate $p \in P$ is the average over all pair-wise similarities between the consecutive windows. Finally, the assigned match for each $q \in Q$ is calculated using argmax over all candidate similarity scores.

Figure 23 presents the average of the results over all modalities for each dataset, respectively. The results verify that observing more frames leads to improved matching results.

8.1. Results: Retrieval through Natural Language

On LIPD-Babel-v2, we evaluate text-to-motion retrieval against TMR++ [2]. For a fair comparison, we run TMR++ only on the subset of Babel that we use in LIPD-Babel-v2. Note that TMR++ has been trained on the full Babel dataset, which gives the model itself an advantage over our model.

Input: Q, K consecutive query/candidate embeddings for respective modality a, b

Output: One-to-Many mapping

```

1 matches  $\leftarrow \emptyset$ 
2 foreach  $q \in Q$  do
3    $match \leftarrow$ 
    $\arg \max_{k \in K} \left( \frac{1}{N} \sum_{n=1}^N \text{sim}(Z_{a,q}^j, Z_{b,k}^j) \right);$ 
4    $matches \leftarrow matches \cup \{match\};$ 
5 end
6 return  $matches$ 

```

Algorithm 1: Matching algorithm for consecutive subsequences

Method	Training Set	R-Top-1
TMR++ Th=0.95	Full Babel	55.54
Ours (Skeleton) Th=0.95	LIPD-Babel-v2	42.55
Ours (Skeleton) Th=0.90		48.92
Ours (IMU) Th=0.95	LIPD-Babel-v2	46.01
Ours (IMU) Th=0.90		46.94
Ours (Pointcloud) Th=0.95	LIPD-Babel-v2	48.68
Ours (Pointcloud) Th=0.90		53.62

Table 5. Text-to-<Skeleton, Pointcloud, IMU> retrieval on LIPD-Babel-v2

The results are presented in Table 5. We use the same threshold (Th) as TMR++ to account for semantically similar retrievals. In addition, we report our results for Th=0.90 and Th=0.95 since the CLIP text embedding space may exhibit different semantic relations compared to the text embeddings used by TMR++. Our results show that our performance is promising, but worse than TMR++, showing possibilities for future work to improve the alignment to text.

9. Ablation Study on LIPD-Babel-v2 for HAR

We perform a large ablation study between all modalities for downstream classification. We ablate linear/non-linear probing and freezing or fine-tuning each model when training for HAR on LIPD-Babel-v2. The results are presented in Table 6 for IMU, Table 7 for point clouds, and Table 8 for skeletons.

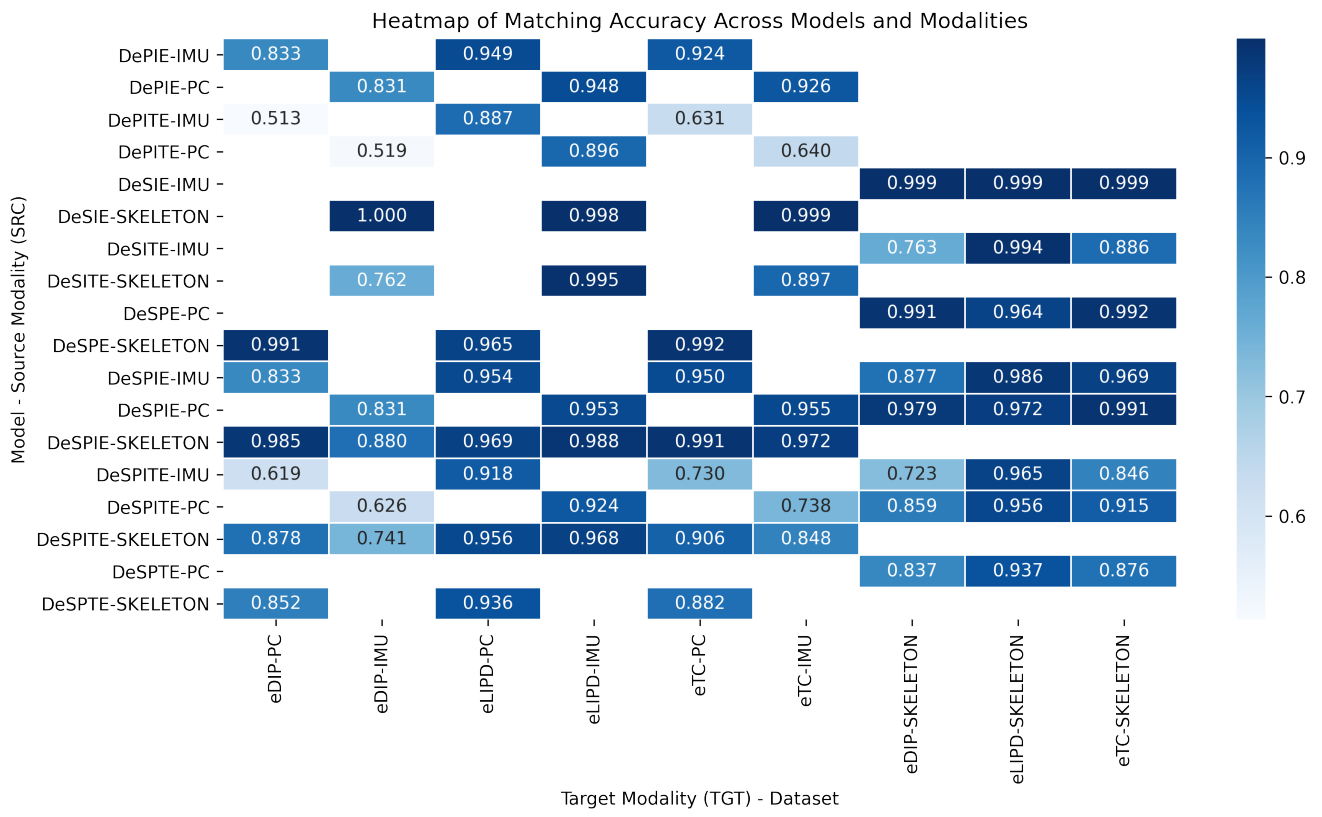


Figure 8. Heatmap to visualize the respective matching results on average across all modalities and datasets at a glance

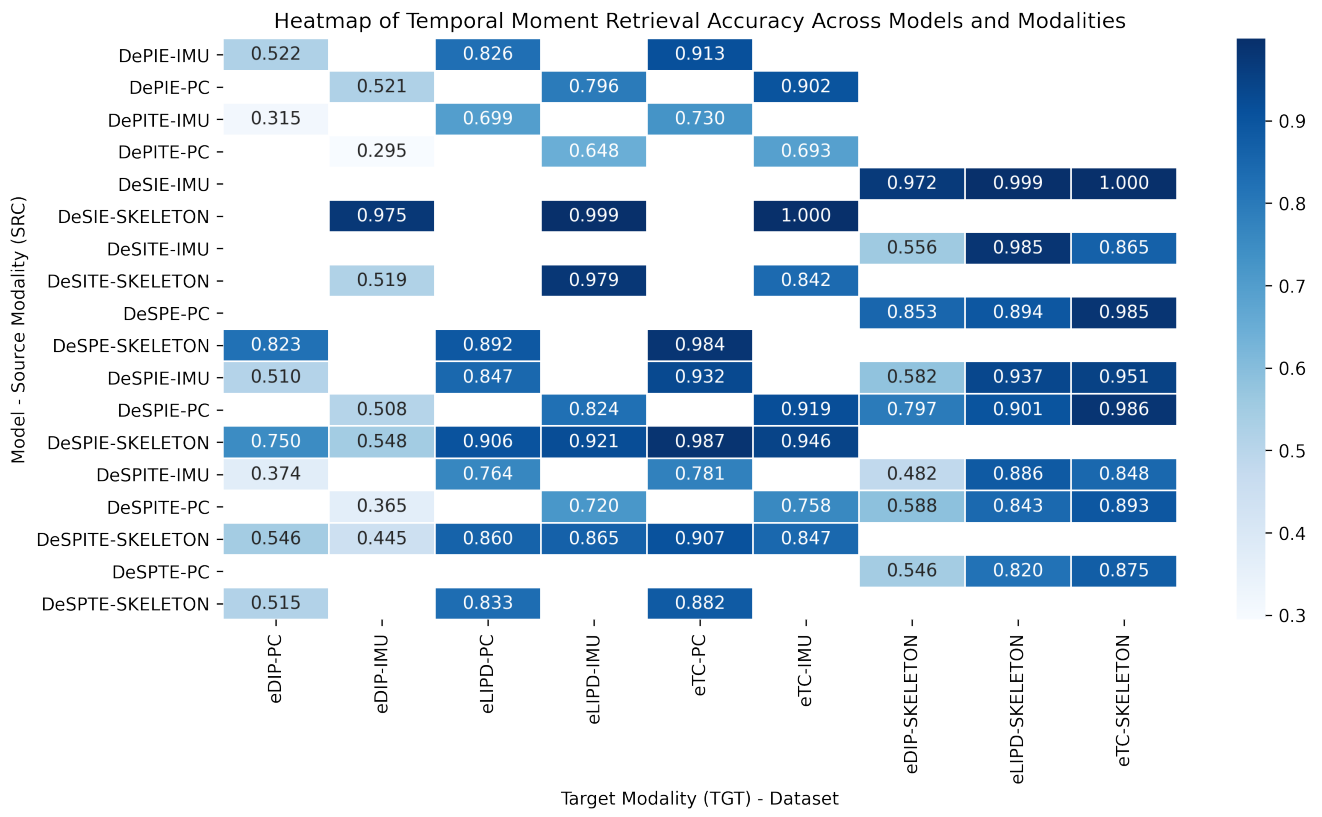


Figure 9. Heatmap to visualize the respective temporal moment retrieval results on average across all modalities and datasets at a glance

Table 6. All IMU HAR classification results on the Babel-LIPD-v2-CLS action recognition dataset, segment-level accuracy $Acc(Seg)$ is reported.

model	Skeleton	PC	IMU	Text	Probing	Fine tuning	Projection Head	$Acc(seg) \uparrow$
Random Init			✓		✓		linear	43.01
Random Init			✓		✓		non-linear	57.12
Random Init			✓			✓	linear	65.62
Random Init			✓			✓	non-linear	64.26
PIE			✓	✓	✓		linear	60.21
PIE			✓	✓	✓		non-linear	62.05
PIE			✓	✓		✓	linear	68.32
PIE			✓	✓		✓	non-linear	67.50
SIE	✓		✓		✓		linear	44.20
SIE	✓		✓		✓		non-linear	56.62
SIE	✓		✓			✓	linear	66.44
SIE	✓		✓			✓	non-linear	67.06
SPIE	✓		✓	✓	✓		linear	58.29
SPIE	✓		✓	✓	✓		non-linear	60.95
SPIE	✓		✓	✓		✓	linear	67.28
SPIE	✓		✓	✓		✓	non-linear	69.21
PITE			✓	✓	✓	✓	linear	61.14
PITE			✓	✓	✓	✓	non-linear	59.21
PITE			✓	✓		✓	linear	68.54
PITE			✓	✓		✓	non-linear	66.63
SITE	✓		✓	✓	✓	✓	linear	56.69
SITE	✓		✓	✓	✓	✓	non-linear	56.95
SITE	✓		✓	✓		✓	linear	66.86
SITE	✓		✓	✓		✓	non-linear	67.10
SPITE	✓		✓	✓	✓	✓	linear	62.06
SPITE	✓		✓	✓	✓	✓	non-linear	59.76
SPITE	✓		✓	✓		✓	linear	68.08
SPITE	✓		✓	✓		✓	non-linear	68.40

Table 7. All point cloud HAR classification results on the Babel-LIPD-v2-CLS action recognition dataset, segment-level accuracy $Acc(Seg)$ is reported.

model	Skeleton	PC	IMU	Text	Probing	Fine tuning	projection	$Acc(seg) \uparrow$
Random Init		✓				✓	linear	65.69
Random Init		✓				✓	non-linear	67.38
Random Init		✓			✓		linear	51.90
Random Init		✓			✓		non-linear	61.98
PIE		✓	✓			✓	linear	65.96
PIE		✓	✓			✓	non-linear	69.52
PIE		✓	✓		✓		linear	68.27
PIE		✓	✓		✓		non-linear	68.36
SPE	✓	✓				✓	linear	66.65
SPE	✓	✓				✓	non-linear	66.13
SPE	✓	✓			✓		linear	63.55
SPE	✓	✓			✓		non-linear	64.17
SPIE	✓	✓	✓			✓	linear	67.51
SPIE	✓	✓	✓			✓	non-linear	66.93
SPIE	✓	✓	✓		✓		linear	67.06
SPIE	✓	✓	✓		✓		non-linear	66.41
SPTE	✓	✓		✓		✓	linear	67.43
SPTE	✓	✓		✓		✓	non-linear	67.30
SPTE	✓	✓		✓	✓		linear	69.31
SPTE	✓	✓		✓	✓		non-linear	68.66
PITE	✓	✓	✓	✓		✓	linear	68.84
PITE	✓	✓	✓	✓		✓	non-linear	69.50
PITE	✓	✓	✓	✓	✓		linear	70.04
PITE	✓	✓	✓	✓	✓		non-linear	69.00
SPITE	✓	✓	✓	✓		✓	linear	69.00
SPITE	✓	✓	✓	✓		✓	non-linear	68.04
SPITE	✓	✓	✓	✓	✓		linear	67.06
SPITE	✓	✓	✓	✓	✓		non-linear	66.32

Table 8. All skeleton HAR classification results on the Babel-LIPD-v2-CLS action recognition dataset, segment-level accuracy $Acc(Seg)$ is reported.

model	Skeleton	PC	IMU	Text	Probing	Fine tuning	projection	$Acc(seg) \uparrow$
Random Init	✓					✓	linear	67.90
Random Init	✓					✓	non-linear	68.23
Random Init	✓				✓		linear	59.71
Random Init	✓				✓		non-linear	60.59
SIE	✓		✓			✓	linear	67.79
SIE	✓		✓			✓	non-linear	70.44
SIE	✓		✓		✓		linear	50.50
SIE	✓		✓		✓		non-linear	57.14
SPE	✓	✓				✓	linear	69.06
SPE	✓	✓				✓	non-linear	70.14
SPE	✓	✓			✓		linear	58.55
SPE	✓	✓			✓		non-linear	59.93
SPIE	✓	✓	✓			✓	linear	68.31
SPIE	✓	✓	✓			✓	non-linear	67.47
SPIE	✓	✓	✓		✓		linear	61.76
SPIE	✓	✓	✓		✓		non-linear	63.64
SPTE	✓	✓		✓		✓	linear	69.20
SPTE	✓	✓		✓		✓	non-linear	69.01
SPTE	✓	✓		✓	✓		linear	65.84
SPTE	✓	✓		✓	✓		non-linear	65.93
SITE	✓		✓	✓		✓	linear	68.14
SITE	✓		✓	✓		✓	non-linear	69.64
SITE	✓		✓	✓	✓		linear	63.83
SITE	✓		✓	✓	✓		non-linear	63.93
SPITE	✓	✓	✓	✓		✓	linear	70.64
SPITE	✓	✓	✓	✓		✓	non-linear	69.91
SPITE	✓	✓	✓	✓	✓		linear	67.20
SPITE	✓	✓	✓	✓	✓		non-linear	66.77

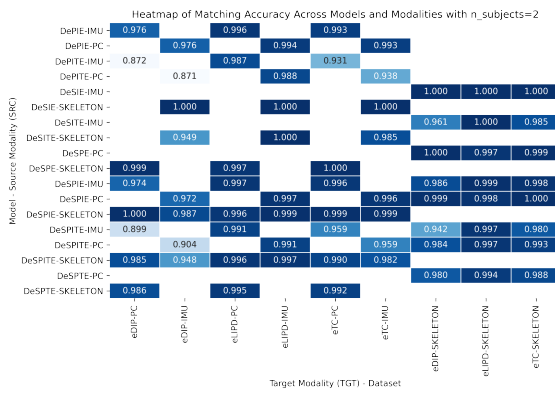


Figure 10. Matching, subjects=2

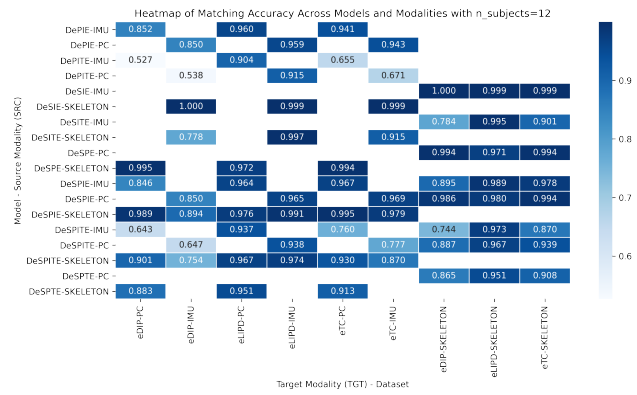


Figure 13. Matching, subjects=12

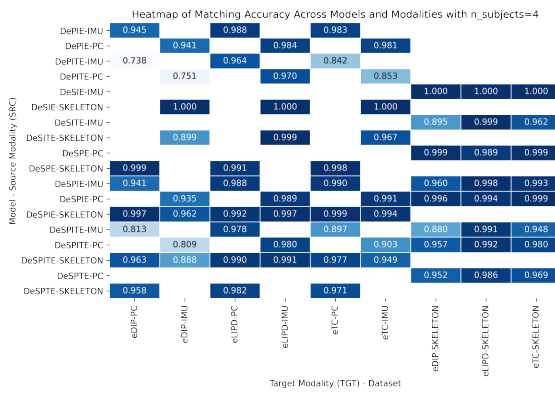


Figure 11. Matching, subjects=4

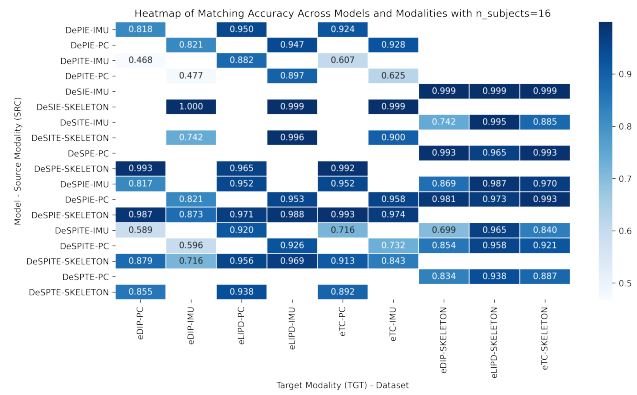


Figure 14. Matching, subjects=16

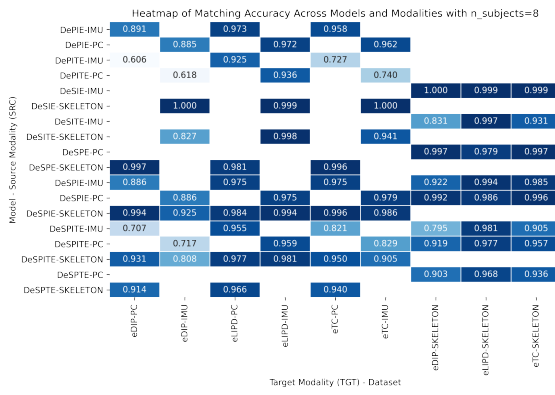


Figure 12. Matching, subjects=8

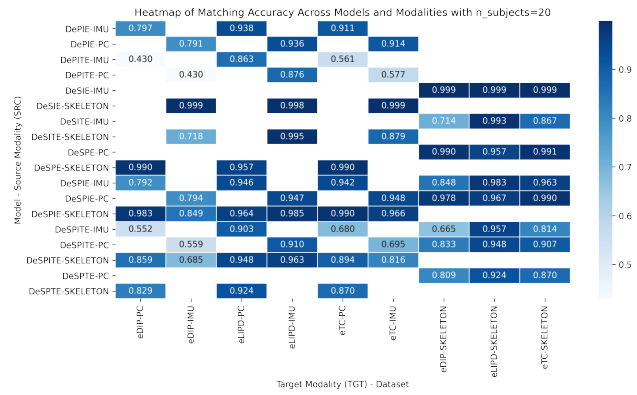


Figure 15. Matching, subjects=20

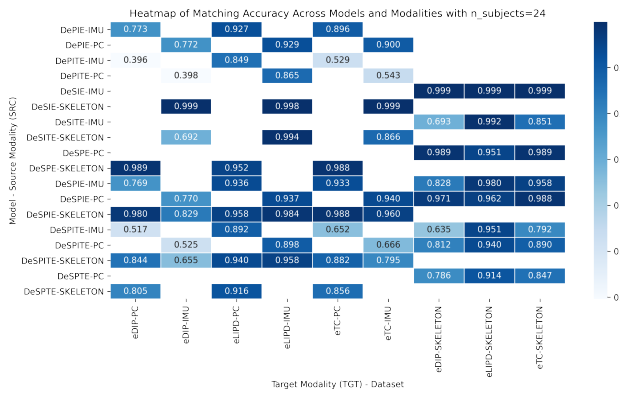


Figure 16. Matching, subjects=24

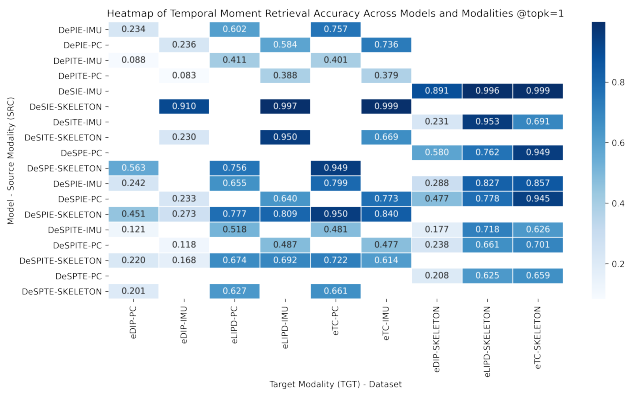


Figure 19. Temporal Moment Retrieval, topk=1

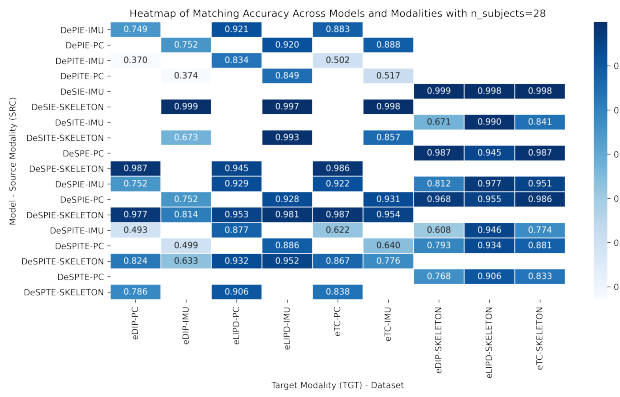


Figure 17. Matching, subjects=28

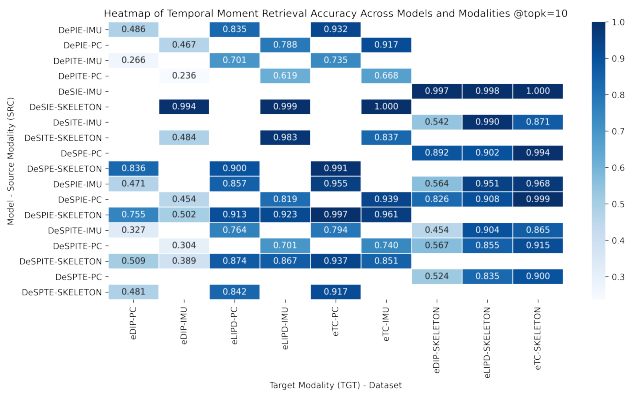


Figure 20. Temporal Moment Retrieval, topk=10

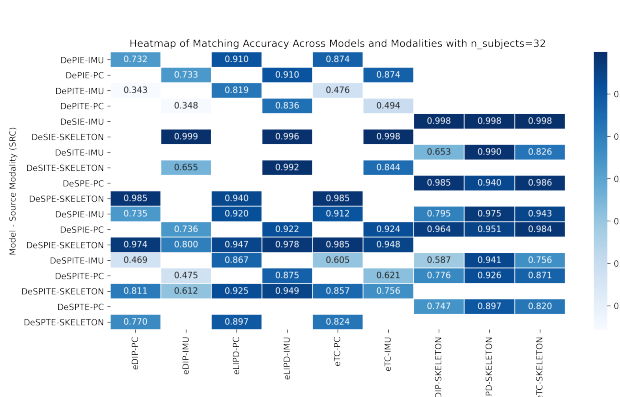


Figure 18. Matching, subjects=32

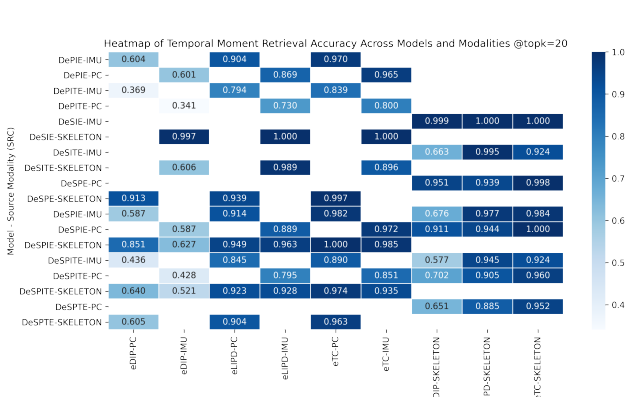


Figure 21. Temporal Moment Retrieval, topk=20

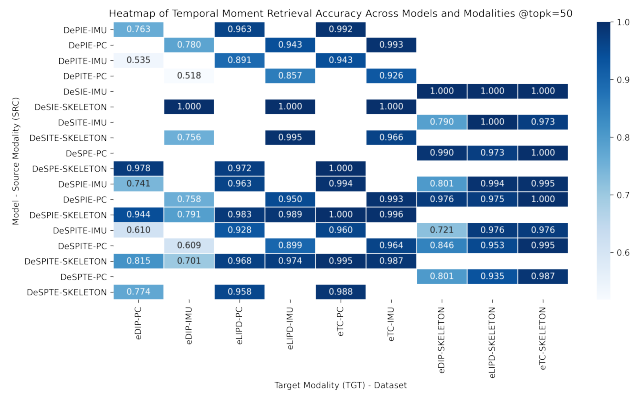


Figure 22. Temporal Moment Retrieval, topk=50

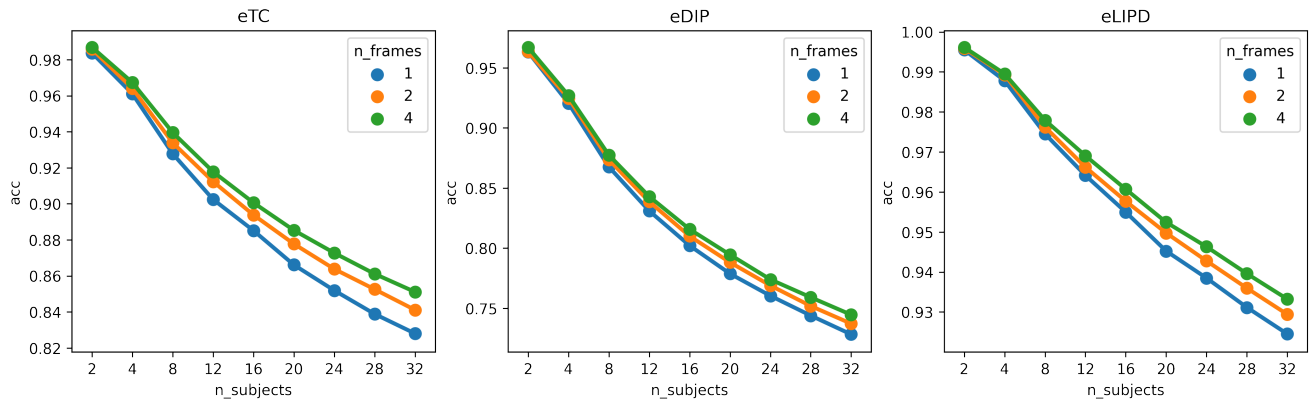


Figure 23. Performance of computing matching scores based on 1,2, or 4 consecutive windows. The matching scores are presented averaged over each model and modality combination to show the effectiveness of matching based on consecutive windows.